7

Phase Shift Functions with Gaussian Decrease

The Gausssian function has a number of appealing properties. It is simple and analytic. It is finite in range, but quite smooth in its behavior. Since it happens also to play a fundamental role in constructing the harmonic oscillator wave functions of the nuclear shell model, it is frequently used to represent the densities of the lightest nuclei. It is sometimes used also to represent the short-range interactions between incident particles and such nuclei. If such an interaction potential, $V(\boldsymbol{r})$, is Gaussian in shape, then the phase shift function $\chi(b)$ given by Eq. (2.5) is a Gaussian function of b. We can write it as

$$\chi_{\mathrm{g}}(b_x, b_y) = A_{\mathrm{g}} \exp(-b^2/\beta^2), \tag{7.1}$$

where $b^2 = b_x^2 + b_y^2$, and the strength parameter A_{g} may, in general, be complex. We shall first study the scattering for this phase shift function in some detail, and then discuss two closely related cases in which the phase shift function varies rather less inside a radius $b = c$, but has a similar Gaussian falloff at larger values of b. These are

$$\chi_l(b_x, b_y) = A_\ell \log\{1 + \exp[(c^2 - b^2)/\beta^2]\}, \tag{7.2}$$

$$\chi_{\mathrm{Fg}}(b_x, b_y) = A_{\mathrm{Fg}}/\{1 + \exp[(c^2 - b^2)/\beta^2]\}. \tag{7.3}$$

They are suggestive, to a degree, of phase shift functions that have been used to represent scattering by nuclei with diffuse surfaces.

For illustrative purposes, we choose the relative normalization

$$A_{\mathrm{Fg}} = A_\ell = A_{\mathrm{g}}/\exp[c^2/\beta^2], \tag{7.4}$$

and compare the three phase shift functions in Fig. 7.1, for $A_{\mathrm{g}} = 3, c = \beta = 1$ fm. At first sight (Fig. 7.1(a), where they are plotted linearly) they appear rather different. However, in a typical case of strong absorption, the central region will not contribute very much to the scattering amplitude; instead it is the edge region which

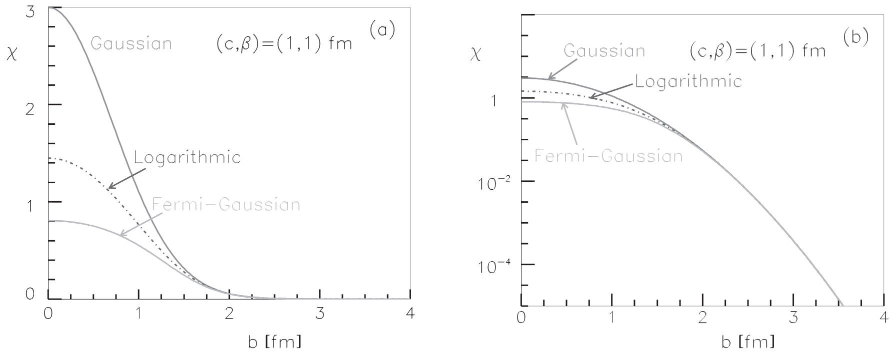

Figure 7.1 Phase shift functions Eqs. (7.1–7.3) with a Gaussian edge. The same three phase shift functions are shown both in linear (a) and logarithmic (b) representations.

is important. This region is better illustrated on a logarithmic scale, in Fig. 7.1(b). With the normalization of Eq. (7.4), the edge region for these three phase shift functions is essentially the same. We will see below, that the differential scattering cross sections will also be rather similar.

Since these phase shift functions are all symmetric under rotation, all the stationary phase points will occur at $b_y = 0$. We will therefore, as in Chapter 5, only need to make use of the function $\chi(b_x, 0)$. It will be convenient therefore to abbreviate it as

$$X(b_x) \equiv \chi(b_x, 0). \tag{7.5}$$

An important difference between the three functions Eqs. (7.1–7.3) is that the Gaussian function $X(b_x)$ is analytic in the entire complex b_x-plane. For the logarithmic case Eq. (7.2) and the "Fermi–Gaussian" Eq. (7.3), on the other hand, the function $X(b_x)$ possesses branch points and poles successively for

$$b_x^2 = c^2 + (2n+1)i\pi\beta^2, \quad n = 0, \pm 1, \pm 2, \ldots \tag{7.6}$$

7.1 The Real-Valued Gaussian Phase Shift Function

For the simple Gaussian phase shift function of Eqs (7.1) and (7.5),

$$X(b_x) = A_{\rm g} \exp(-b_x^2/\beta^2), \tag{7.7}$$

the stationary points are determined by Eq. (5.2) or

$$X'(b_x) = -2(b_x/\beta^2) A_{\rm g} \exp(-b_x^2/\beta^2) = q. \tag{7.8}$$

It is instructive, before letting A_{g} take on complex values, to consider the case of real A_{g} in some detail. The behavior of the scattering is similar in some ways to that of the simplified model we considered in Section 4.3. It will furnish us with another example of the "rainbow" phenomenon, an angle at which the differential cross section, as we have approximated it, becomes singular. This time, however, we shall go a step further in the approximation procedure and show how the improvement removes the singularity.

To find stationary points we can begin by squaring both sides of Eq. (7.8). If we let

$$Z = \frac{b_x^2}{\beta^2} \tag{7.9}$$

and

$$\mu = \frac{q\beta}{2A_{\mathrm{g}}}, \tag{7.10}$$

then the resulting relation can be written as

$$Ze^{-2Z} = \mu^2. \tag{7.11}$$

For real Z, the expression Ze^{-2Z} has a maximum value $(2e)^{-1}$ at $Z = \frac{1}{2}$. Eq. (7.11) has two real, positive roots, for $0 \le \mu^2 \le (2e)^{-1}$. One has $Z < \frac{1}{2}$ and the other $Z > \frac{1}{2}$. Two possible roots for b_x,

$$b_x = \pm\beta\sqrt{Z} \tag{7.12}$$

will correspond to each of the roots for Z, but squaring Eq. (7.8) has in fact given us twice as many roots as we need. Half of them are spurious. It is easy to see that for $A_{\mathrm{g}} > 0$, i.e. an attractive potential, only the negative roots for b_x will actually satisfy Eq. (7.8). Likewise, for $A_{\mathrm{g}} < 0$, only the positive roots will do.

Let us assume, for definiteness, that $A_{\mathrm{g}} > 0$, and that the parameter μ lies in the interval $0 \le \mu \le (2e)^{-\frac{1}{2}}$, so that we have

$$0 \le q \le \frac{A_{\mathrm{g}}}{\beta}\sqrt{\frac{2}{e}}. \tag{7.13}$$

If we write the two roots of Eq. (7.11) as $Z_1 \ge \frac{1}{2}$ and $Z_2 \le \frac{1}{2}$, the stationary points we seek are given by (the index β is being reserved for the stationary point $b_{\beta\,x}$, to be defined below)

$$b_{\alpha\,x} = -\beta\sqrt{Z_1} \le -\frac{\beta}{\sqrt{2}} \tag{7.14a}$$

$$b_{\gamma\,x} = -\beta\sqrt{Z_2} \ge -\frac{\beta}{\sqrt{2}}. \tag{7.14b}$$

As q is increased to the upper bound in the inequality Eq. (7.13) the two stationary points $b_{\alpha x}$ and $b_{\gamma x}$ coalesce at the value $-\beta/\sqrt{2}$, which is analogous to the value $b_{x,\mathrm{R}}$ of Section 4.3. We therefore expect a rainbow singularity to appear in the approximated differential cross section at the q-value

$$q_{\mathrm{R}} = \frac{A_{\mathrm{g}}}{\beta}\sqrt{\frac{2}{e}}. \tag{7.15}$$

At the stationary points we have

$$X(b_{jx}) = A_{\mathrm{g}} e^{-Z_j} = -\frac{q\beta^2}{2b_{jx}} \tag{7.16}$$

$$X''(b_{jx}) = -\frac{2A_{\mathrm{g}}}{\beta^2}(1-2Z_j)e^{-Z_j} = \frac{q}{b_{jx}}\left(1 - 2\frac{b_{jx}^2}{\beta^2}\right) \tag{7.17}$$

The integration Eq. (3.4) may then be carried out along the real b_x-axis. We find that the two stationary points, as in Eq. (3.23), yield the two contributions

$$f_j(\boldsymbol{k}', \boldsymbol{k}) = \frac{k}{i}\left\{\frac{-b_{jx}}{qX''(b_{jx})}\right\}^{\frac{1}{2}} e^{i[-qb_{jx}+X(b_{jx})]} \quad (j = \alpha, \gamma) \tag{7.18a}$$

$$= \frac{k\beta}{iq}\left\{\frac{-b_{jx}^2}{\beta^2 - 2b_{jx}^2}\right\}^{\frac{1}{2}} e^{-iqb_{jx}(1+\beta^2/2b_{jx}^2)}. \tag{7.18b}$$

For $q > q_{\mathrm{R}}$, both of the stationary points move off the real axis, but only one of them moves into the lower half-plane, to furnish a convergent integral over the coordinate b_y. To find that stationary point we note that it still obeys Eq. (7.11). Our problem then is to find where in the complex Z-plane the expression Ze^{-2Z} can take on real, positive values. If we let

$$Z = re^{i\theta} \tag{7.19}$$

then Eq. (7.11) becomes

$$re^{i(\theta - 2r\sin\theta) - 2r\cos\theta} = \mu^2, \tag{7.20}$$

and since the expression Ze^{-2Z} must be real-valued we see that the root must lie on the curve

$$2r\sin\theta = \theta \tag{7.21}$$

or

$$r = \frac{\theta}{2\sin\theta}. \tag{7.22}$$

The point $\theta = 0$, $r = \frac{1}{2}$, for example, corresponds to the rainbow point $Z = \frac{1}{2}$. When we substitute this back in Eq. (7.20) we find the equation

$$\mu^2 = \frac{\theta}{2\sin\theta} e^{-\theta\cot\theta}. \tag{7.23}$$

The expression on the right is a monotonically increasing function of θ for $0 \leq \theta \leq \pi$ that rises to ∞ from the rainbow value of $1/2e$. If θ is a positive root of this equation we can write Z, using Eqs. (7.19) and (7.22), as

$$Z_+ = \tfrac{1}{2}(\theta\cot\theta + i\theta), \quad \theta > 0. \tag{7.24}$$

The stationary point that we seek then for $A_g > 0$ is given by

$$b_{1x} = -\beta\sqrt{Z_+}. \tag{7.25}$$

We have had to choose the negative branch of the square root, as before, since the positive root is a false one. If the interaction had the opposite sign, on the other hand, it would have been appropriate to use the positive root, and in that case we would need the negative root of Eq. (7.23) for θ.

There are other stationary points in the lower half-plane, but as in the example considered in Chapter 5, we have no need to use them at this stage or even find them. We can carry out the integration, as in our prior examples, by translating the path into the lower half-plane and passing it through the single stationary point we have just found. Then the values of $X(b_x)$ and $X''(b_x)$ at the stationary point are again given by Eqs. (7.16) and (7.17). It is worth noting that for $q > q_R$, the function X'', evaluated as in Eq. (7.17), has a positive imaginary part. The integrand, as indicated, for example, in Eqs. (3.18a) and (3.21b), has a Gaussian decrease to either side of the stationary point. By passing the contour through the stationary point along a horizontal path, in other words, we are integrating through a maximum of the modulus, and, in a sense, using a compromise between the methods of stationary phase and steepest descent. To the extent that the contribution of a stationary point is approximated by a convergent straight-line integral of the sort we have used, all of these compromises corresponding to different directions of the path furnish the same result. It is not too material then which of the names we attach to the method. But, however we choose to approximate the stationary point contributions, it is worth pointing out one conceptual advantage of the method of steepest descents. It furnishes us an excellent determination of a path for crossing the complex plane by traversing whatever stationary points are necessary for an asymptotic approximation. We can use the path of steepest descent as a guide to the significant stationary points, and then approximate their contribution much as we have been doing.

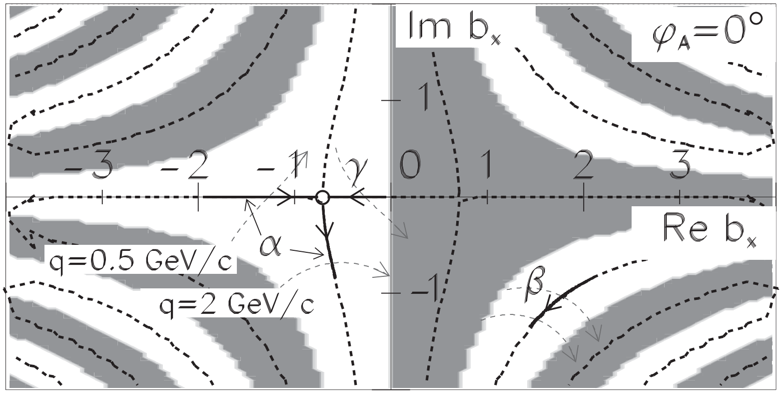

Figure 7.2 Trajectories of stationary points for $X_{\mathrm{g}}(b) = A_{\mathrm{g}} \exp(-b^2/\beta^2)$, with $A_{\mathrm{g}} = |A_{\mathrm{g}}| \exp(i\varphi_A)$, for the real case, $\varphi_A = 0°$. The scale parameter β is chosen as the unit of length. These trajectories are shown in the complex b_x-plane, where $\boldsymbol{b} = (b_x, b_y)$. The thinly dashed curves indicate paths of integration. (At the stationary points, $b_y = 0$.)

In order to develop some better understanding of how the integrand varies in the complex b_x-plane, and of the approximations involved, we display in Fig. 7.2 some properties of $X'(b_x)$. Even without the explicit formulas for the stationary points given above, one can easily determine graphically where they are constrained to lie. Our sign convention is such that stationary-phase points can only occur where $\mathrm{Re}\, X'(b_x) > 0$. As a first step, the complex b_x-plane is therefore divided into regions where $\mathrm{Re}\, X'(b_x) > 0$ (white) alternating with regions where $\mathrm{Re}\, X'(b_x) < 0$ (shaded). Next, we note that at the stationary points, $X'(b_x)$ must be purely real. Thus, we also show the locations where $\mathrm{Im}\, X'(b_x)$ vanishes. These are the dashed lines running along the white and shaded "bands", roughly in their middle, including in this case the negative, real axis. From the above discussion, it is now clear that stationary points can only be found along those dashed lines that run somewhere near the middle of the *white* bands. It may be noted that these are independent of the strength of the interaction, but they do of course depend on the phase; in this example A_{g} is real.

Indeed, the "trajectories", given by Eq. (5.2) above, which are the paths in the complex b_x-plane, followed by the stationary points as functions of the momentum transfer, q, are shown as solid segments along such dashed lines. Here, the strength of the interaction plays a role, as does the momentum transfer. On the negative real axis, we identify the points α and γ. The segments shown correspond to the range in momentum transfer 0.1 GeV/c $\leq q \leq$ 3 GeV/c. The rainbow point, where for real A_{g} the trajectories α and γ run together, is shown as an open circle.

Paths of integration corresponding to $A_{\mathrm{g}} = 5$ are shown schematically for $q = 0.5$ and 2 GeV/c (thinly dashed). For the purpose of this illustration, these are determined by mapping out the path of steepest descent on each side of the stationary point. It now becomes clear, that in order to continue the path of integration out to $\mathrm{Re}\, b_x = \infty$, more "ridges" have to be passed. The dominant one of these, β, is also shown. The contribution from this stationary point will be omitted in our discussion of the cross section for the real Gaussian, but it will become more prominent when in Section 7.3 we consider complex interactions, $\mathrm{Im}\, A_g > 0$.

The single stationary point on the integration path for $q > q_R$ yields a scattering amplitude of the same general form Eq. (7.18b) as those for $q < q_R$. Like both of those, it also possesses a singularity at the rainbow point $q = q_R$. For $q < q_R$ the amplitudes furnished by the two stationary points interfere. For $q > q_R$, on the other hand, there is only one such amplitude and it decreases rapidly in modulus as q increases further.

To evaluate our scattering amplitude numerically we should note that their dependence on the four parameters k, q, A_g, and β possesses a certain scale invariance. Because $f(\boldsymbol{k}', \boldsymbol{k})$ is simply proportional to k, and A_g is dimensionless we can write

$$f(\boldsymbol{k}', \boldsymbol{k}) = k\beta^2 \Phi(q\beta, A_g), \tag{7.26}$$

where Φ is the same function for all phase shifts that can be expressed in the Gaussian form, Eq. (7.1). If we write the differential cross section, furthermore in the form

$$\frac{\mathrm{d}\sigma}{\mathrm{d}q^2} = \frac{\pi}{k^2}\frac{\mathrm{d}\sigma}{\mathrm{d}\Omega} = \frac{\pi}{k^2}|f(\boldsymbol{k}', \boldsymbol{k})|^2, \tag{7.27}$$

that has become customary in high-energy elementary particle physics, then we have

$$\frac{\mathrm{d}\sigma}{\mathrm{d}q^2} = \pi\beta^4 |\Phi(q\beta, A_g)|^2. \tag{7.28}$$

In that case $\beta^{-4}\,\mathrm{d}\sigma/\mathrm{d}q^2$ becomes simply a function of two parameters.

We have graphed the differential cross section $\mathrm{d}\sigma/\mathrm{d}q^2$ for $A_g = 5$, 10, and 15, and for $\beta = 1$ fm, in Figs. 7.3(a)–(c). We have adopted the value of the momentum as $k = 1.7$ GeV/c, corresponding to $T_{\mathrm{kin}} = 1$ GeV, and recall that $[\beta = 1\ \mathrm{fm}]^{-1}$ corresponds to a momentum transfer of 0.197 GeV/c.

The dashed curves on the same plots are the differential cross sections for the same parameters that result from a more direct numerical integration of the diffraction amplitude, which, according to Eq. (2.2), is given by

$$f(\boldsymbol{k}', \boldsymbol{k}) = ik\int_0^\infty J_0(qb)\left\{1 - e^{i\chi(b)}\right\} b\,\mathrm{d}b, \quad q = |\boldsymbol{k}' - \boldsymbol{k}|. \tag{7.29}$$

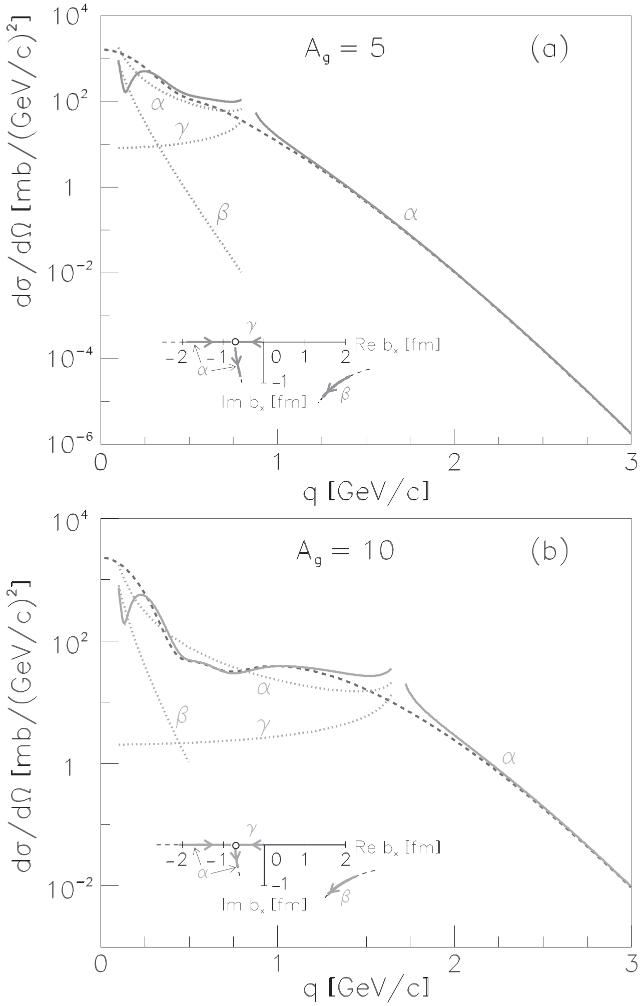

Figure 7.3 Differential cross sections for $\chi_g(b) = A_g \exp(-b^2/\beta^2)$, with A_g real; (a) $A_g = 5$, (b) $A_g = 10$, (c) $A_g = 15$ (next page). The scale parameter β is 1 fm. The inserts show the trajectories of stationary points for the range in momentum transfer 0.02 GeV/c $\leq q \leq$ 6 GeV/c (dotted). The parts of the trajectories that correspond to the cross section plots, 0.1 GeV/c $\leq q \leq$ 3 GeV/c, are indicated as solid curves. The arrows indicate the sense in which the stationary points move as the momentum transfer increases. The differential cross sections contributed by each of the stationary points, α, β, and γ, are shown as dotted curves. The trajectory γ contributes only out to the rainbow point. The solid curves show the resulting cross section, evaluated in the asymptotic approach (rainbow singularities occur at the discontinuities), whereas the dashed curves show the results of numerical evaluations of the diffraction integrals.

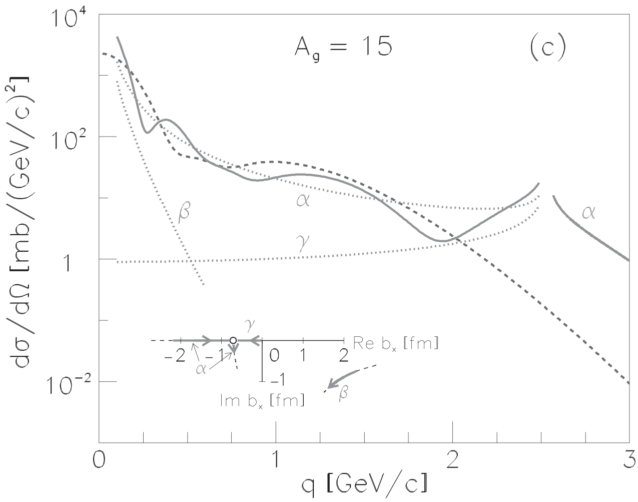

Figure 7.3 (c) See caption to parts (a) and (b) on previous page.

For a phase shift function that has a restricted range, as is the case with the Gaussian, this integral is easily evaluated, and the agreement is seen to be excellent, except for q-values in two limited ranges. One of these is the range of small q-values, $q\beta \ll 1$, to which the asymptotic approximation simply does not apply. The other is the region near the rainbow point q_R, where the approximation becomes singular, and the true cross section is not (for the three values of A_g, the rainbow points are located at 0.85, 1.70, and 2.54 GeV/c). We shall discuss the behavior near the rainbow point a bit further shortly, but let us first note some of the broader features of these results.

The wavy appearance of the differential cross section for $q < q_R$, i.e., inside the rainbow, clearly results from the interference of the amplitudes provided by the two stationary points on the real b_x-axis. For $q > q_R$, on the other hand the smooth falloff is due to the amplitude contributed by the single stationary point. As we have noted earlier, it is the exponential function in the amplitude Eq. (7.18b) that dominates its q-dependence; the other factors have a much weaker dependence on q. The squared modulus of this exponential function alone yields

$$|f_j(\boldsymbol{k}', \boldsymbol{k})|^2 \sim \exp\left\{2q \,\mathrm{Im}\left[b_{jx}\left(1 + \frac{\beta^2}{2b_{jx}^2}\right)\right]\right\}. \tag{7.30}$$

Since the stationary point for $q > q_R$ has $\mathrm{Im}\, b_x$ negative, and since $|b_{jx}|^2 > \frac{1}{2}\beta^2$ we can recognize a rate of decrease that is essentially exponential in q. Of course the stationary point b_x itself will also depend somewhat on the value of q, so we can say a bit more about the q-dependence of the expression Eq. (7.30) by seeing how $\operatorname{Im} b_{j\,x}$ varies for large q. For quite large momentum transfers, $q \gg q_{\mathrm{R}}$, the root of Eq. (7.23) is

$$\theta \sim \pi\left(1 - \frac{1}{2\log\mu}\right), \tag{7.31}$$

which shows that

$$Z_{+} \sim -\log\mu + \frac{i\pi}{2}, \tag{7.32}$$

and

$$\begin{aligned}\operatorname{Im} b_x &\sim -\beta\sqrt{\log\mu} \\ &\sim -\beta\sqrt{\log\left(\frac{q\beta}{2A_{\mathrm{g}}}\right)}.\end{aligned} \tag{7.33}$$

The differential cross section should therefore show a very slow increase in its logarithmic slope with increasing q, and that is indeed evident in the graphs.

7.2 Differential Cross Section near the Rainbow Point

Our approximation to the differential cross section, as we have seen, diverges at the rainbow point $q = q_{\mathrm{R}}$. That is because our method of approximation is an asymptotic one, valid in the limit of short wavelengths. In the limit of zero wavelength there is indeed a sharp singularity in the physical cross section, but the approach to that limit is slow. For the cases we have graphed $\beta q_{\mathrm{R}} = A_{\mathrm{g}}\sqrt{2/e}$ ranges from only 4.3 to 12.9, and the numerically integrated diffraction amplitude shows little hint of that behavior. For such modest values of βq_{R}, therefore, there may be some value in correcting our approximation procedure, at least in the neighborhood of the rainbow point.

Our problem is to find a more sensitive way of carrying out the integration Eq. (3.4) when the stationary points on which we have thus far based it are quite near the point $b_{x,\mathrm{R}}$ at which

$$X''(b_{x,\mathrm{R}}) = \frac{\partial^2}{\partial b_x^2}\chi(b_x, 0)\bigg|_{b_x = b_{x,\mathrm{R}}} = 0. \tag{7.34}$$

Since the function $\chi(b)$ is rotationally invariant, its value for any b_x is stationary as a function of b_y for $b_y = 0$. We can always expand $\chi(b_x, b_y)$ about $b_y = 0$ and carry out the b_y integration as we did in Eq. (3.21a). It is the integration over b_x that we shall have to improve. We can do that by expanding $X(b_x) = \chi(b_x, 0)$ not about the stationary points we have used before, but instead about the point $b_{x,\mathrm{R}}$ at which X'' vanishes. If we carry out this expansion to third order we have

$$X(b_x) = X(b_{x,\mathrm{R}}) + (b_x - b_{x,\mathrm{R}})X'(b_{x,\mathrm{R}}) + \tfrac{1}{6}(b_x - b_{x,\mathrm{R}})^3 X'''(b_{x,\mathrm{R}}). \tag{7.35}$$

The integral that we must evaluate is then of the form

$$J(q) = \lim_{\epsilon \to 0} \int_{-\infty}^{\infty} \exp\{-\epsilon b_x^2 + i\xi(b_x - b_{x,\mathrm{R}}) + i\eta(b_x - b_x R)^3\} \, \mathrm{d}b_x, \tag{7.36}$$

which is convergent for $\epsilon \to 0$. If we shift the coordinate b_x we can then write

$$J(q) = 2 \int_0^{\infty} \cos\{\eta b_x^3 + \xi b_x\} \, \mathrm{d}b_x. \tag{7.37}$$

The coeffficients η and ξ in this expression are given by

$$\xi = q - X'(b_{x,\mathrm{R}}) = q - q_\mathrm{R} \tag{7.38}$$

$$\eta = -\tfrac{1}{6} X'''(b_{x,\mathrm{R}}). \tag{7.39}$$

We have here made use of the fact that the integrand in Eq. (7.37) is unchanged under a simultaneous change of sign of η and ξ, and reversed the signs of both η and ξ in the identification above.

The integral Eq. (7.37) is an Airy function [1],

$$J(q) = \frac{2\pi}{(3\eta)^{\frac{1}{3}}} \,\mathrm{Ai}\left(\frac{\xi}{(3\eta)^{\frac{1}{3}}}\right). \tag{7.40}$$

Its behavior is not at all singular at the rainbow point. The full scattering amplitude in this approximation is given by

$$f(\boldsymbol{k}', \boldsymbol{k}) = \frac{k}{i} \left\{\frac{2\pi i b_{x,\mathrm{R}}}{q}\right\}^{\frac{1}{2}} \left(\frac{2}{-X'''(b_{x,\mathrm{R}})}\right)^{\frac{1}{3}} \mathrm{Ai}\left[(q - q_\mathrm{R})\left(\frac{2}{-X'''(b_{x,\mathrm{R}})}\right)^{\frac{1}{3}}\right]$$
$$\times\, e^{-iqb_{x,\mathrm{R}} + iX(b_{x,\mathrm{R}})}. \tag{7.41}$$

The Cartesian derivative of $X(b_x)$ in this expression can be written in terms of radial derivatives of $\chi(b)$ for real values of b_x as

$$X'''(b_x) = \frac{b_x}{|b_x|} \chi'''(|b_x|). \tag{7.42}$$

Since the expression Eq. (7.41) for the scattering amplitude is based on an expansion about the point $b_{x,\mathrm{R}}$, which is $\beta/\sqrt{2}$ for the Gaussian phase shift, it can not be expected to hold over a broad range of q-values. As we can see from the differential cross section curves shown in Fig. 7.4, the expression based on our third order expansion does remove the singularity at the rainbow point, and substantially improves the asymptotic approximation in the region about it.[1]

[1] The Airy result represents the contributions from the stationary points α and γ. The contribution of the β trajectory would give some additional contribution inside the rainbow.

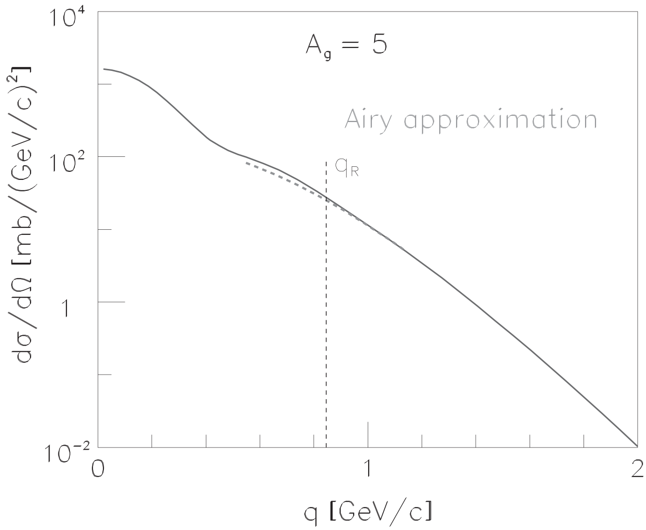

Figure 7.4 Differential cross sections for $\chi_g(b) = A_g \exp(-b^2/\beta^2)$, with $A_g = 5$ and $\beta = 1$ fm. The solid curve shows the results of a numerical integration of the diffraction integral, while the dashed curve shows the result of the Airy approximation.

While we have taken some pains to correct the asymptotic approximation in the neighborhood of the rainbow points, we should note that such corrections are not often necessary. Rainbow points are rarities in the complex plane. They tend to occur only for real-valued phase shift functions, and then only on the real axis. When $X(b_x)$ is a complex-valued analytic function, its second derivative, i.e., both real and imaginary parts, will not in general vanish at any of the stationary points we have defined earlier. It follows then, that rainbow scattering, as we have defined it, tends not to occur in the purely nuclear domain. However, as we shall see in Chapters 11 and 12, for scattering from an extended charge, without or even with additional nuclear interactions, there may be rainbow phenomena implicit.

7.3 Gaussian Phase Shift Function with Absorption

When absorption is present, we must let A_g become complex,

$$A_g = |A_g| e^{i\varphi_A}, \quad 0 \le \varphi_A \le \pi . \tag{7.43}$$

Also in this more general case, the stationary points are determined by Eq. (7.8), but the solutions $b_{j\,x}$ will now be complex, even for small values of the momentum transfer. By taking the logarithms on both sides of Eq. (7.8), the equation for the stationary points can then be written as

$$b_{j\,x}^2 = \beta^2\left[\log\left(\frac{2A_g}{q\beta}\right) + \log\left(\frac{-b_{j\,x}}{\beta}\right)\right]. \tag{7.44}$$

If we further write $b_{j\,x}$ as

$$b_{j\,x} = |b_{j\,x}|e^{i\varphi}, \quad -\pi \le \varphi \le 0, \tag{7.45}$$

then Eq. (7.44) is equivalent to

$$\cos(2\varphi) + \frac{\sin(2\varphi)}{2[\varphi_A + \varphi + (2n+1)\pi]}\left\{\log\left(\frac{\sin(2\varphi)}{2[\varphi_A + \varphi + (2n+1)\pi]}\right) - \log\left[2\left(\frac{|A_g|}{q\beta}\right)^2\right]\right\} = 0, \quad \text{with } n = 0, \pm 1, \pm 2, \ldots, \tag{7.46}$$

and with

$$b_{j\,x} = \beta\sqrt{\left|\frac{\varphi_A + \varphi + (2n+1)\pi}{\sin(2\varphi)}\right|}\,e^{i\varphi}. \tag{7.47}$$

We note that Eq. (7.44) for the complex variable $b_{j\,x}$ has effectively been reduced to an equation for *one* real variable φ, since Eq. (7.46) is independent of the modulus $|b_{j\,x}|$. The relationship, Eq. (7.47), between the phase φ and the modulus $|b_{j\,x}|$ is independent of $|A_g|$ and q, in agreement with the general statements, Eqs. (3.5) and (7.8).

Points of stationary phase are shown in Fig. 7.5 for $\varphi_A = 30^\circ$ and 90°; compare Eq. (7.43). It is instructive to compare this with Fig. 7.2 for the real case. We note that, whereas the remaining points of stationary phase in the third quadrant, $b_{\alpha\,x}$, have moved downward, those in the fourth quadrant, $b_{\beta\,x}$, have moved upward by a similar distance. While the stationary point in the fourth quadrant was of little importance for real, positive A_g, since it was far from the real axis, it begins to increase in importance as φ_A increases. When $\varphi_A = 90^\circ$, the stationary points $b_{\alpha\,x}$ and $b_{\beta\,x}$ are situated symmetrically with respect to the imaginary axis, $b_{\beta\,x} = -b_{\alpha\,x}^*$. This is a consequence of the Schwarz reflection symmetry obeyed by $f_j(\boldsymbol{k}', \boldsymbol{k})$, and leads to

$$f_\beta(\boldsymbol{k}', \boldsymbol{k}) = -f_\alpha^*(\boldsymbol{k}', \boldsymbol{k}), \quad \varphi_A = 90^\circ, \tag{7.48}$$

in agreement with the more general result, Eq. (2.11).

These changes in the behavior of the stationary points play an essential role in explaining the changing structure of the cross section as a function of φ_A. Two such differential cross sections and the positions of the associated stationary points are shown in Fig. 7.6. For $\varphi_A < 90^\circ$, the contributions from $b_{\alpha\,x}$ and $b_{\beta\,x}$ are seen to be quite different,

$$|f_\beta(\boldsymbol{k}', \boldsymbol{k})| < |f_\alpha(\boldsymbol{k}', \boldsymbol{k})|, \tag{7.49}$$

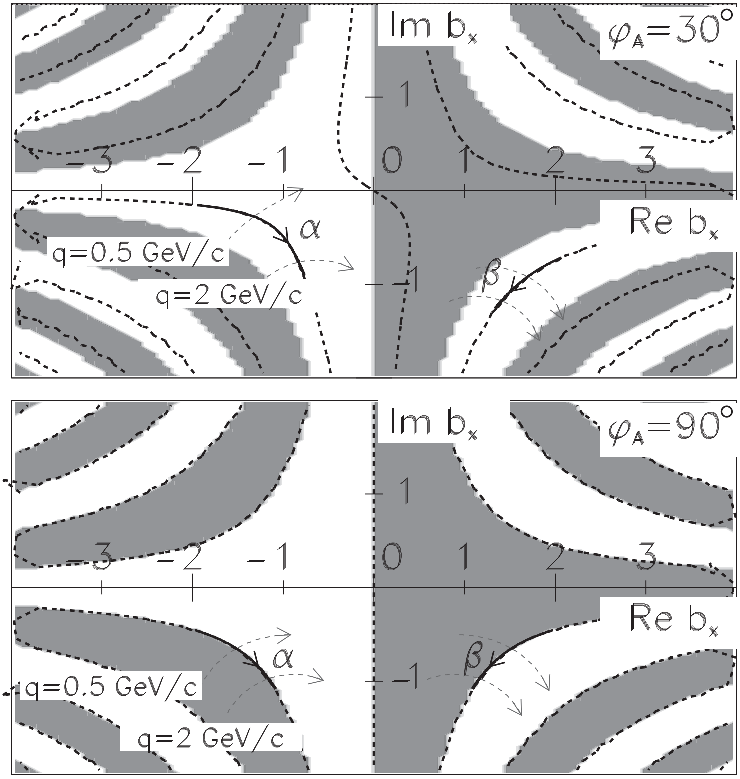

Figure 7.5 Trajectories of stationary points for $X_{\mathrm{g}}(b) = A_{\mathrm{g}} \exp(-b^2/\beta^2)$, with $A_{\mathrm{g}} = |A_{\mathrm{g}}| \exp(i\varphi_A)$, for two values of φ_A: 30° and 90°. Similar to Fig. 7.2.

with $|f_\alpha(\boldsymbol{k}', \boldsymbol{k})|^2$ becoming the dominant contribution to the cross section as $q \to \infty$. On the other hand, for $\varphi_A = 90°$, the two contributions are equal in magnitude [cf. Eq. (7.48)]; the differential cross section has zeros when they interfere destructively.

The variation of the phase of each term with increasing momentum transfer is roughly given by $q \operatorname{Re} b_{j\,x}$. This leads to a regular diffractive interference pattern, with period determined by

$$\Delta q = \frac{\pi}{\left|\operatorname{Re}\left\{b_{\alpha\,x} - b_{\beta\,x} + \dfrac{1}{q}\left[X(b_{\beta\,x}) - X(b_{\alpha\,x})\right]\right\}\right|}$$
$$= \frac{\pi}{\left|\operatorname{Re}\left\{b_{\alpha\,x}\left[1 + \dfrac{\beta^2}{2|b_{\alpha\,x}|^2}\right] - b_{\beta\,x}\left[1 + \dfrac{\beta^2}{2|b_{\beta\,x}|^2}\right]\right\}\right|}. \tag{7.50}$$

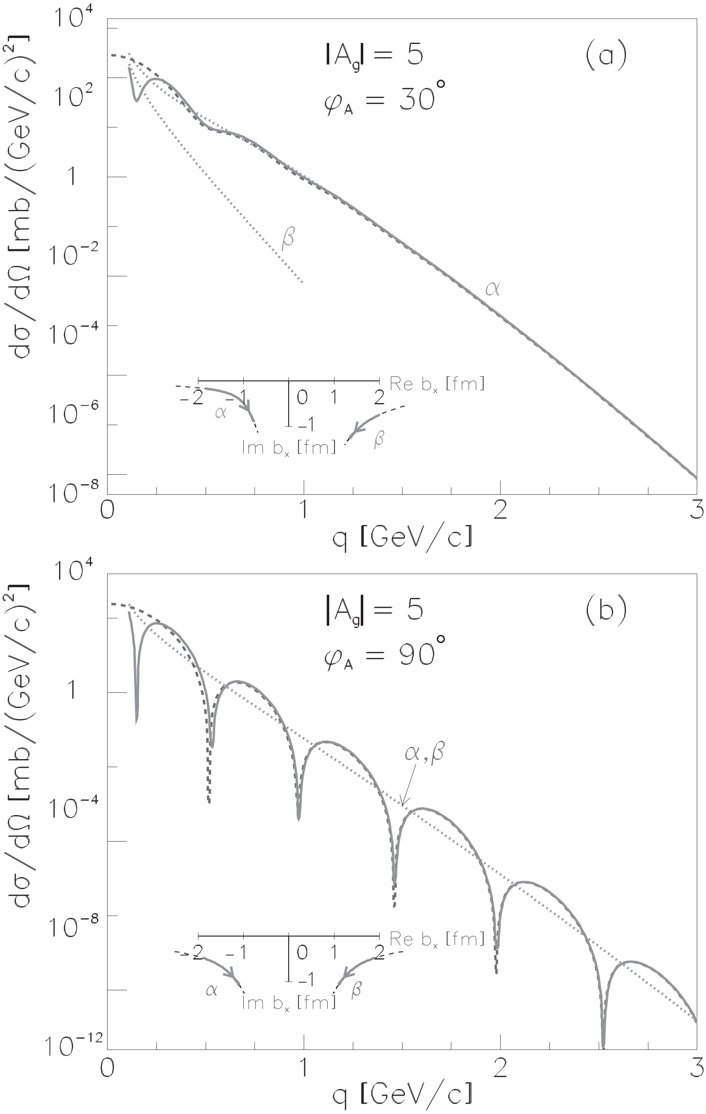

Figure 7.6 Differential cross sections for $\chi_g(b) = A_g \exp(-b^2/\beta^2)$, with $A_g = |A_g| \exp(i\varphi_A)$, $\beta = 1$ fm and $|A_g| = 5$; (a) $\varphi_A = 30°$, (b) $\varphi_A = 90°$. As in Fig. 7.3, the inserts show the trajectories of stationary points, and their individual contributions to the differential cross sections are shown as dotted curves. The results of numerical evaluations of the diffraction integrals are shown as dashed curves.

Asymptotically, the period of oscillation will change very slowly, according to

$$|\operatorname{Re} b_{j\,x}| \simeq \frac{\pi\beta}{2}\left[\log\left(\frac{q\beta}{2|A_{\mathrm{g}}|}\right) + \mathcal{O}\left(\log\log\left(\frac{q\beta}{2|A_{\mathrm{g}}|}\right)\right)\right]^{-1/2}, \quad (\text{for } \varphi_A = \pi/2). \tag{7.51}$$

Asymptotically, the contribution to the amplitude from each region of stationary phase, $b_{j\,x}$, decreases with increasing q roughly as

$$|f_j(\boldsymbol{k}', \boldsymbol{k})| \sim \exp\left\{q \operatorname{Im} b_{j\,x}\left[1 - \frac{\beta^2}{2|b_{j\,x}|^2}\right]\right\}, \tag{7.52}$$

since the remaining factors have a much weaker q-dependence. The fact that $\operatorname{Im} b_{\alpha\,x}$ is negative and decreases further with increasing q, accounts for the steepening slope of the cross section for $q > q_{\mathrm{R}}$. In fact, asymptotically, we find that

$$\operatorname{Im} b_{j\,x} \simeq -\beta\left[\log\left(\frac{q\beta}{2|A_{\mathrm{g}}|}\right) + \mathcal{O}\left(\log\log\left(\frac{q\beta}{2|A_{\mathrm{g}}|}\right)\right)\right]^{-1/2}, \tag{7.53}$$

and the slope of the cross section will thus increase rather slowly.

In Fig. 7.7 we compare the cross sections obtained for purely absorptive interactions of different strengths. These correspond to the three values of $|A_{\mathrm{g}}| = 1$, 5,

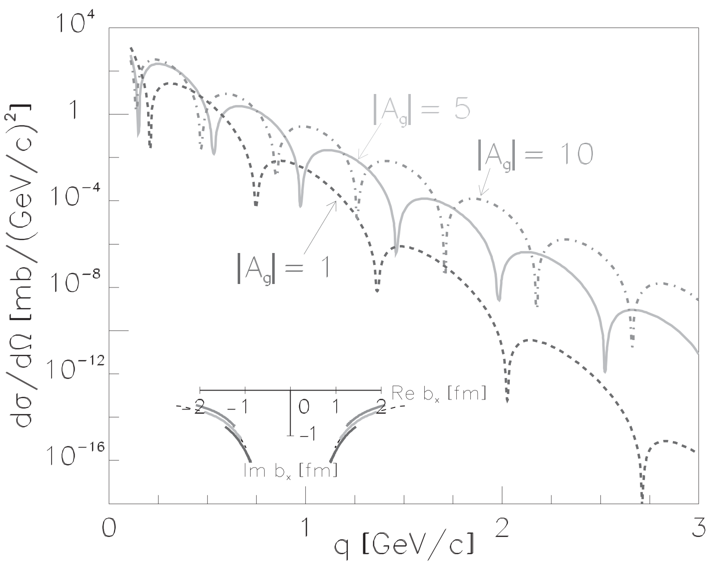

Figure 7.7 Differential cross sections for $\chi_{\mathrm{g}}(b) = i|A_{\mathrm{g}}|\exp(-b^2/\beta^2)$, for $\beta = 1$ fm. Three values of $|A_{\mathrm{g}}|$ are considered: 1, 5, and 10. The locations of the stationary points (those for $|A_{\mathrm{g}}| = 1$ and 10 are a little offset vertically, for clarity), and the periods and slopes of the envelopes of the differential cross sections are seen to depend on the strengths of the interaction in an essential fashion.

and 10, and $\varphi_A = 90^\circ$ in all three cases. The different periods of oscillation can be understood in terms of Eq. (7.50): the stronger the absorption, the shorter the period of oscillation, in terms of q. Also, for stronger absorption, the slope of the cross section envelope is seen to undergo a decrease, since asymptotically,

$$\operatorname{Im} b_{jx} \simeq -\beta\left[\log\left(\frac{q\beta}{2|A_{\mathrm{g}}|}\right) + \mathcal{O}\left(\log\log\left(\frac{q\beta}{2|A_{\mathrm{g}}|}\right)\right)\right]^{-1/2}. \tag{7.54}$$

The relationship between the classical concept of force and the condition of stationary phase [cf. Eq. (3.5)], is a particularly simple one for the Gaussian phase shift function. The potential corresponding to the Gaussian phase shift function, Eq. (7.1), is readily found from Eq. (2.6c) to be

$$V(\boldsymbol{b}, z) = -\frac{\hbar v}{\sqrt{\pi}\beta}\,\chi(\boldsymbol{b})e^{-z^2/\beta^2}, \tag{7.55}$$

where v is the projectile velocity. At the point of stationary phase, where $\nabla\chi(\boldsymbol{b})\big|_{\boldsymbol{b}=\boldsymbol{b}_j} = \boldsymbol{q}$, the transverse component of the force, $\boldsymbol{F}_t$, is given by

$$\boldsymbol{F}_t(\boldsymbol{b}_j, z) = -\boldsymbol{\nabla}_{\boldsymbol{b}} V(\boldsymbol{b}, z)\big|_{\boldsymbol{b}=\boldsymbol{b}_j} = \frac{v}{\sqrt{\pi}\beta}\boldsymbol{q}\, e^{-z^2/\beta^2}, \tag{7.56}$$

and the value of the potential according to Eq. (7.16) may be written as

$$V(\boldsymbol{b}_j, z) = \frac{v\beta}{2\sqrt{\pi}}\,\frac{\boldsymbol{q}\cdot\boldsymbol{b}_j^*}{|\boldsymbol{b}_j|^2}\, e^{-z^2/\beta^2}. \tag{7.57}$$

Three remarks are here in order:

i. The deflective force, $\boldsymbol{F}_t$, is real along the entire path, $-\infty < z < \infty$, of stationary phase. This is a special property of the Gaussian potential, for which the dependence on transverse and longitudinal coordinates factorizes.
ii. A real potential, Eq. (7.55), will acquire an absorptive part at the stationary impact parameter if that point lies off the real axis, $\operatorname{Im} b_{jx} < 0$. That explains why the cross section tends to fall exponentially beyond the rainbow point, $q > q_{\mathrm{R}}$.
iii. The sign of the real part of the potential for the path corresponding to the stationary impact vector $\boldsymbol{b}_j$ is determined by $\operatorname{Re}(\boldsymbol{q}\cdot\boldsymbol{b}_j)$. Thus, the sign of $\operatorname{Re} V(\boldsymbol{b}_j, z)$ may differ from its value taken for real arguments, given by Eq. (7.55). Two complex paths can thus pass through opposite sides of the nucleus (i.e., with opposite signs of $\operatorname{Re} b_x$), but still lead to the same point of observation. The effective potential, given by Eq. (7.57), can thus be attractive on one side of the nucleus and repulsive on the other. That is in fact why there can be two such opposite trajectories that contribute interfering amplitudes for a given momentum transfer.

Much of the remainder of this Chapter 7 deals with phase shift functions with Gaussian edges, and the somewhat flatter central dependence of Eqs. (7.2) and (7.3). It may be considered as background material that can be skipped in a first reading, in order to focus on other significant features of the phase shift function.

7.4 Logarithmic Phase Shift Function

We consider next the logarithmic phase shift function of Eq. (7.2),

$$\chi_l(b_x, b_y) = A_\ell \log\{1 + \exp[(c^2 - b^2)/\beta^2]\}. \tag{7.58}$$

The equation for the stationary points, $\nabla\chi(\boldsymbol{b}) = \boldsymbol{q}$ can be reduced to

$$\begin{aligned} b_{j\,x}^2 &= c^2 + \beta^2 \log\left[-1 - \frac{2b_{j\,x}A_\ell}{q\beta^2}\right] \\ &= c^2 + \beta^2\left\{(2n+1)i\pi + \log\left[1 + \frac{2b_{j\,x}A_\ell}{q\beta^2}\right]\right\}, \quad \text{for } n = 0, \pm 1, \pm 2, \ldots \end{aligned} \tag{7.59}$$

Asymptotically, as $q \to \infty$ the relevant solutions will approach the logarithmic singularities of $\chi_l(b_x)$ that are located at

$$b_x = \pm\sqrt{c^2 \mp i\pi\beta^2}. \tag{7.60}$$

Eq. (7.59) can easily be solved by using the iteration method discussed in Appendix B, starting at these singularities.

At the stationary points, we have

$$\begin{aligned} X_l(b_{j\,x}) &= -A_\ell \log\left(1 + \frac{q\beta^2}{2b_{j\,x}A_\ell}\right), \\ X_l''(b_{j\,x}) &= -\frac{2qb_{j\,x}}{\beta^2}\left(1 - \frac{\beta^2}{2b_{j\,x}^2} + \frac{q\beta^2}{2b_{j\,x}A_\ell}\right). \end{aligned} \tag{7.61}$$

For an appropriate choice of parameters, the edge of the phase shift function Eq. (7.58) will be the same as that of the Gaussian, i.e., we have

$$X_l(b_x \gg c) \simeq X_{\mathrm{g}}(b_x), \tag{7.62}$$

provided

$$A_\ell\, e^{c^2/\beta^2} = A_{\mathrm{g}}, \quad \beta_l = \beta_{\mathrm{g}} = \beta. \tag{7.63}$$

At small momentum transfers, only the edge of the phase shift function is relevant for the scattering amplitudes. This may be seen quantitatively as follows: if $q\beta/A_\ell$ is sufficiently small, Eq. (7.59) for the stationary points reduces to

Eq. (7.44) which applies for the Gaussian case. The points of stationary phase will thus be the same for the two phase shift functions. It is also readily seen from Eq. (7.61) that for small values of $q\beta/A_\ell$, $X_l(b_{jx})$ and $X_l''(b_{jx})$ will become the same as $X_g(b_{jx})$ and $X_g''(b_{jx})$, respectively. The amplitudes will thus be the same for sufficiently small values of $q\beta/A_\ell$ in the two cases.

At large momentum transfers, however, the two phase shift functions will lead to differential cross sections that are considerably different. Because of the presence of a (logarithmic) singularity, X_l will lead to a more stable pattern of oscillations than that resulting from X_g. This increased stability is illustrated in Fig. 7.8 where we compare the cross sections which correspond to X_l and X_g, for two positions of the singularity.

As a common reference, we have in Fig. 7.8(a) chosen the differential cross section resulting from X_g with $A_g = 3i$ and $\beta = 1$ fm. The parameters considered in Fig. 7.8(a) are such that the singularity is at

$$b_x = \pm\sqrt{1 \mp i\pi}\ \text{fm} \quad (\text{or, equivalently}, c = 1\ \text{fm}),$$

whereas those considered in Fig. 7.8(b) are such that the singularity is at

$$b_x = \pm\sqrt{-1 \mp i\pi}\ \text{fm} \quad (\text{or, equivalently}, c = i\ \text{fm}).$$

As explained above, the angular distributions for the two phase shift functions coincide at small momentum transfers. For larger momentum transfers, however, the two phase shift functions lead to quite different cross sections. The cross section corresponding to χ_l acquires a more slowly varying, asymptotically constant, period of oscillation,

$$\Delta q = \frac{\pi}{2\,\mathrm{Re}\sqrt{c^2 - i\pi\beta^2}}, \tag{7.64}$$

and similarly a more slowly varying, asymptotically constant, slope of the envelope,

$$2\left|\mathrm{Im}\sqrt{c^2 - i\pi\beta^2}\right|. \tag{7.65}$$

These different ways in which the period of oscillation, and the slope of the envelope change with momentum transfer for the two cases, are related to the variation of the stationary points with momentum transfer. The stationary points for the Gaussian and the logarithmic phase shift functions are compared in the small graphs inserted in Fig. 7.8. For the logarithmic phase shift function the stationary points approach the singularities in the complex b_x-plane, located at $\pm 1.466 - 1.072i$ fm and $\pm 1.072 - 1.466i$ fm, respectively, for the two sets of parameters. Thus, from Eqs. (7.64) and (7.65) it follows that the period of oscillation will be shorter by about 30% and the slope of the cross section envelope will also be smaller by about 30% than in the second case. This may be seen from a comparison of the cross

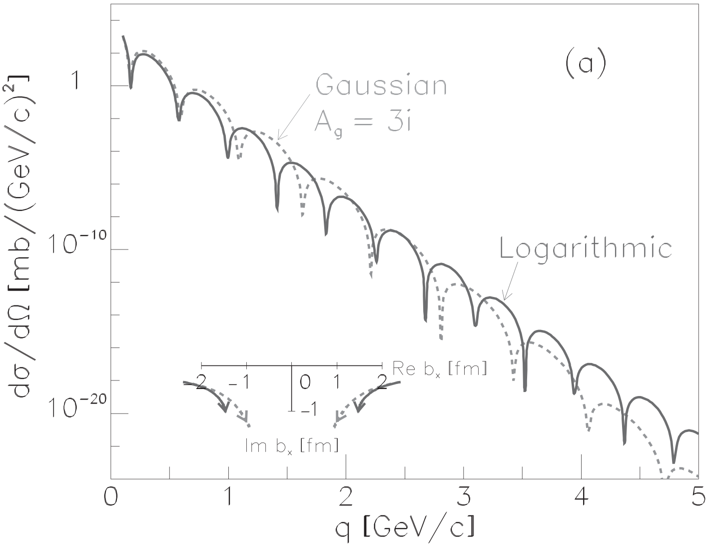

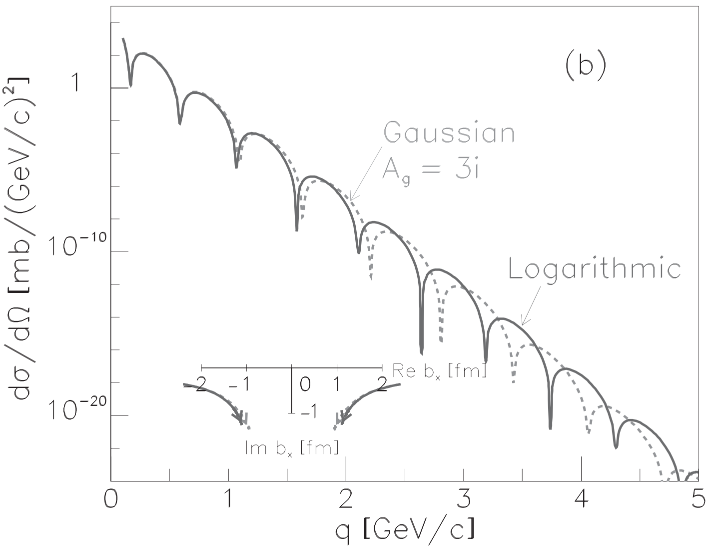

Figure 7.8 Comparisons of the differential cross sections resulting from two phase shift functions having equal edges, $\chi_g(b) = A_g \exp(-b^2/\beta^2)$ and $\chi_l(b) = A_\ell \log\{1 + \exp[(c^2 - b^2)/\beta^2]\}$. The parameters are chosen such that $A_g = A_\ell \exp(c^2/\beta^2) = 3i$, and $\beta = 1$ fm. Two positions are considered for the logarithmic singularity, (a) $b_x = \pm\sqrt{1 \mp i\pi}$ fm (or $c = 1$ fm), (b) $b_x = \pm\sqrt{-1 \mp i\pi}$ fm (or $c = i$ fm). The differential cross sections and the trajectories of stationary points corresponding to χ_g are shown as dashed curves, whereas those corresponding to χ_l are shown as solid curves.

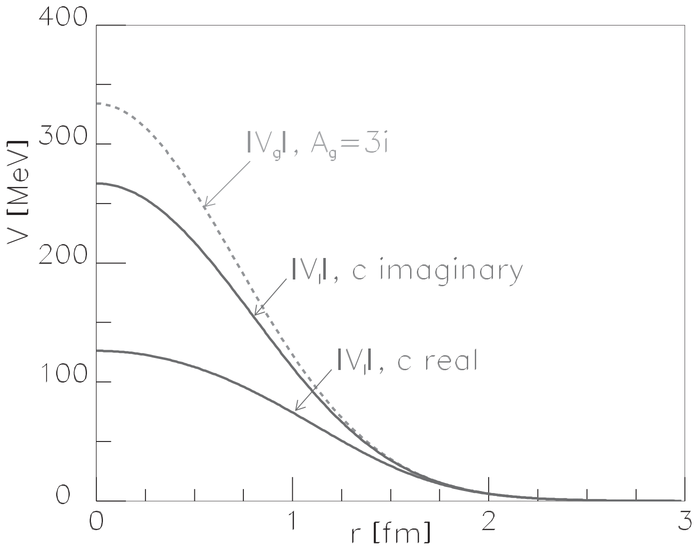

Figure 7.9 Moduli of the potentials corresponding to the Gaussian and logarithmic phase shift functions considered in Fig. 7.8.

sections given in Fig. 7.8(a) and (b), using the cross section for the Gaussian phase shift as a common reference.

It is also instructive to compare the potentials $V_{\mathrm{g}}(r)$ and $V_l(r)$ that correspond to $X_{\mathrm{g}}(b_x)$ and $X_l(b_x)$, respectively. The potential $V_{\mathrm{g}}(r)$ was given in Eq. (7.55), which we rewrite as

$$V_{\mathrm{g}}(r) = -\frac{v A_{\mathrm{g}}}{\sqrt{\pi}\beta} e^{-r^2/\beta^2}, \tag{7.66}$$

whereas $V_l(r)$ may be determined from the Abel equation [cf. Eq. (2.6a)],

$$V_l(r) = -\frac{2vA_\ell}{\pi\beta^2} \int_0^\infty \mathrm{d}\xi \left[1 + e^{(r^2-c^2+\xi^2)/\beta^2}\right]^{-1}. \tag{7.67}$$

These potentials are graphed in Fig. 7.9, for the sets of parameters presented in Fig. 7.8. They are seen to be identical at large values of r, but to differ considerably for small r.

7.5 "Fermi–Gaussian" Phase Shift Function

The third phase shift function we consider with a Gaussian edge is the "Fermi–Gaussian" of Eq. (7.3),

$$\chi_{\mathrm{Fg}}(b_x, b_y) = A_{\mathrm{Fg}}/\{1 + \exp[(b^2 - c^2)/\beta^2]\}. \tag{7.68}$$

Like the logarithmic one, $X_{\rm Fg}(b_x)$ also has singularities at

$$b_x^2 = \pm\sqrt{c^2 \mp i\pi\beta^2}. \tag{7.69}$$

The equation for the stationary points,

$$-\frac{2b_x}{\beta^2}\frac{A_{\rm Fg}E}{(1+E)^2} = q, \tag{7.70}$$

with

$$E \equiv \exp[(b_x^2 - c^2)/\beta^2], \tag{7.71}$$

may be solved by the method outlined in Appendix B. As $q \to \infty$, the solutions will approach the singularities, given by Eq. (7.69). But $X_{\rm Fg}$ has pole singularities, whereas X_l has logarithmic singularities; as a consequence the stationary points approach the singularities at different rates in the two cases.

In order to discuss the asymptotic properties of the differential cross section, let us write the solution to Eq. (7.70) as

$$b_x^2 = c^2 + \beta^2[(2n+1)i\pi + \log(\bar{E})], \tag{7.72}$$

with

$$\bar{E} = 1 + \frac{A_{\rm Fg}b_x}{q\beta^2} + \left[\frac{2A_{\rm Fg}b_x}{q\beta^2} + \left(\frac{A_{\rm Fg}b_x}{q\beta^2}\right)^2\right]^{1/2}. \tag{7.73}$$

Asymptotically, i.e., for small $|A_{\rm Fg}|/q\beta$, the solution may be approximated as

$$b_x = \pm\left\{c^2 \mp \beta^2\left[i\pi - \left(\frac{2A_{\rm Fg}b_x}{q\beta^2}\right)^{1/2}\right]\right\}^{1/2}, \tag{7.74}$$

where we have chosen the signs such as to give the relevant branches of the multivalued expressions Eqs. (7.72 and 7.73). If we now denote the relevant singular points in the third and fourth quadrants as

$$\begin{aligned} b_x^{(s,\alpha)} &= -\sqrt{c^2 + i\pi\beta^2}, \\ b_x^{(s,\beta)} &= \sqrt{c^2 - i\pi\beta^2}, \end{aligned} \tag{7.75}$$

then we have asymptotically

$$\begin{aligned} b_x^{(\alpha)} &= b_x^{(s,\alpha)} + i\beta\left(\frac{A_{\rm Fg}}{-2qb_x^{(s,\alpha)}}\right)^{1/2}, \\ b_x^{(\beta)} &= b_x^{(s,\beta)} + \beta\left(\frac{A_{\rm Fg}}{2qb_x^{(s,\beta)}}\right)^{1/2}. \end{aligned} \tag{7.76}$$

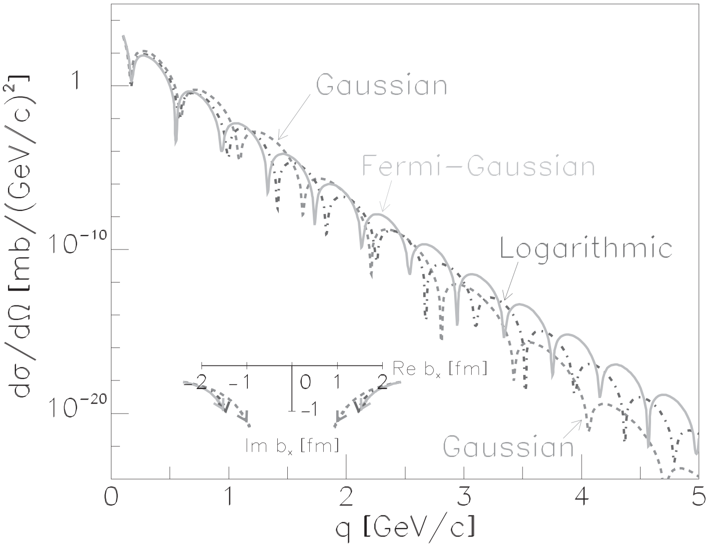

Figure 7.10 Differential cross sections resulting from three phase shift functions that coincide at large impact parameters, but have different analytic properties, $\chi_g(b) = A_g \exp(-b^2/\beta^2)$ (dashed), $\chi_l(b) = A_\ell \log\{1+\exp[(c^2-b^2)/\beta^2]\}$ (dash-dotted), and $\chi_{Fg}(b) = A_{Fg}/\{1+\exp[(b^2-c^2)/\beta^2]\}$ (solid). The parameters satisfy Eq. (7.78). Further, $A_g = 3i$, $\beta = 1$ fm, and $c = 1$ fm (as in Fig. 7.8(a)). The trajectories of stationary points are given in the insert.

For the logarithmic phase shift function, the approach to the singularity is faster. A similar expansion of Eq. (7.59) furnishes the asymptotic relations

$$b_{\alpha x} = b_x^{(s,\alpha)} - \frac{A_\ell}{q},$$
$$b_{\beta x} = b_x^{(s,\beta)} + \frac{A_\ell}{q}. \tag{7.77}$$

Comparing Eqs. (7.76) and (7.77), we also note that the singularities are approached from different directions for the two phase shift functions. This has some bearing on the relative rates at which the envelope and the period of the differential cross section change as functions of momentum transfer.

We show in Fig. 7.10 a comparison of the differential cross sections resulting from X_g, X_l, and X_{Fg}, for pure absorption, and with relative strengths chosen such that the phase shift functions coincide at large impact parameters,

$$A_{Fg}\, e^{c^2/\beta^2} = A_\ell\, e^{c^2/\beta^2} = A_g, \tag{7.78}$$

compare Eq. (7.63). With this condition satisfied, it is easy to show that the differential cross section resulting from X_{Fg} at small momentum transfers coincides with

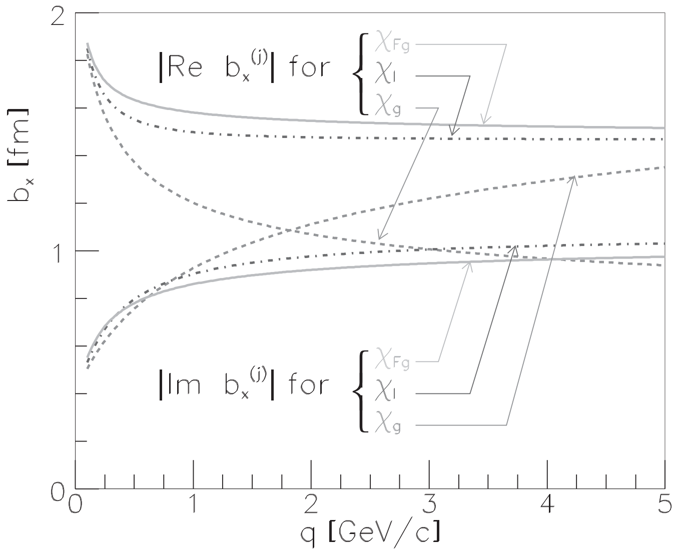

Figure 7.11 Variation of stationary phase coordinates b_{jx} with momentum transfers, for the three phase shift functions considered in Fig. 7.10. The moduli of the real and imaginary parts are shown separately.

those corresponding to the Gaussian and logarithmic phase shift functions. This is seen to be the case in Fig. 7.10, where we have taken the same parameters as in Fig. 7.8(a), i.e., $A_g = 3i$, $\beta = c = 1$ fm.

As the momentum transfer increases, the period of the differential cross section for X_{Fg} is seen to be even more stable than it was for the logarithmic phase shift function. This is largely due to the slower approach of the stationary points to the singularities, as given by Eqs. (7.76) and (7.77) for the two cases. For the parameters considered in Fig. 7.10, the actual q-dependence of the stationary points is shown in Fig. 7.11 for these three phase shift functions.

The differential cross sections corresponding to X_l and X_{Fg} both appear at large momentum transfers to oscillate with nearly constant periods, but to be shifted by half a period with respect to one another. One may determine the way in which the periods approach constancy by evaluating, in addition to the stationary points, the phase shift functions at the stationary points.

At the stationary points, by using $\bar{E}$ defined by Eq. (7.73) we may write

$$X_{Fg}(b_{jx}) = -\frac{q\beta^2}{2b_{jx}}(1 - \bar{E}^{-1}), \tag{7.79}$$

and

$$X''_{Fg}(b_{jx}) = -\frac{2qb_{jx}}{\beta^2}\left[\frac{\bar{E}+1}{\bar{E}-1} - \frac{\beta^2}{2b_{jx}^2}\right]. \tag{7.80}$$

As $q \to 0$, these expressions are seen to become identical to those for the Gaussian phase shift function, as is required for the cross sections to coincide.

Asymptotically, it follows that

$$X_{\mathrm{Fg}}(b_{jx}) \simeq -\left(\frac{q\beta^2 A_{\mathrm{Fg}}}{2b_{jx}}\right)^{1/2}, \tag{7.81}$$

whereas [compare Eq. (7.61)]

$$X_l(b_{jx}) \simeq -A_\ell \log\left(\frac{q\beta^2}{2b_{jx}A_\ell}\right). \tag{7.82}$$

We may combine these results with those for the stationary points, Eqs. (7.76) and (7.77), and obtain thus for the case of pure absorption the dominant q-dependences of the periods:

For X_l:

$$\Delta q \simeq \frac{\pi}{2\,\mathrm{Re}\left[b_x^{(s,\beta)} + \frac{A_\ell}{q}\log\left(\frac{\beta}{2b_x^{(s,\beta)}A_\ell}\right)\right]}, \tag{7.83}$$

for X_{Fg}:

$$\Delta q \simeq \frac{\pi}{2\,\mathrm{Re}\left[b_x^{(s,\beta)} + \beta\left(\frac{2A_{\mathrm{Fg}}}{qb_x^{(s,\beta)}}\right)^{1/2}\right]}. \tag{7.84}$$

(A_ℓ and A_{Fg} are here assumed to be purely imaginary.)

Since the periods of the differential cross sections for the logarithmic and the "Fermi–Gaussian" phase shifts approach their asymptotically constant values at different rates, the phase of one oscillatory pattern will drift with respect to that of the other. At the largest momentum transfers considered in Fig. 7.10, they are shifted by half a period. This shift would increase if the cross sections were followed out to still larger momentum transfers.

For these regularly oscillating differential cross sections, it is useful to introduce the concept of envelopes as the smooth curves to which the differential cross section curves are tangential (analogous to the straight lines in Fig. 1.1). If we denote the exponential slopes of these envelopes by $S(q)$, then the differential cross sections fall as $\exp[-S(q)q]$. The slopes of these envelopes of the cross sections may be determined in a fashion similar to that of the periods discussed above. We thus find:

For X_l:

$$S(q) \simeq 2\left|\,\mathrm{Im}\left\{b_x^{(s,\beta)} + \frac{A_\ell}{q}\left[1 + \log\left(\frac{q\beta^2}{2b_x^{(s,\beta)}A_\ell}\right)\right]\right\}\right|, \tag{7.85}$$

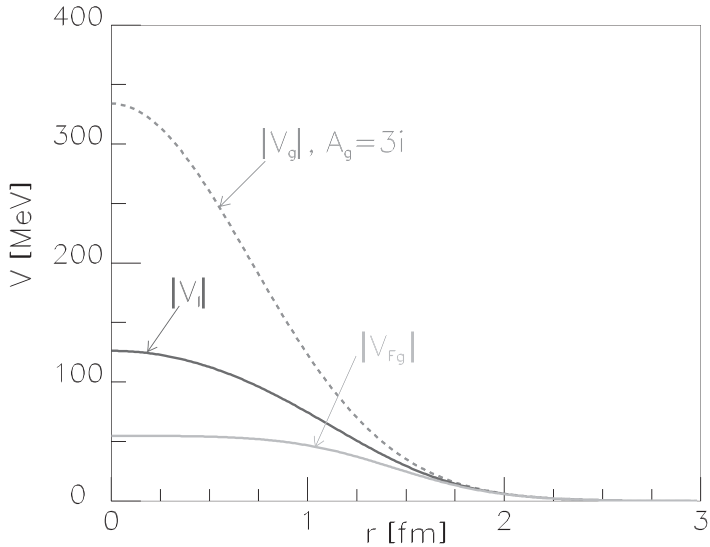

Figure 7.12 Moduli of the potentials corresponding to the Gaussian, logarithmic, and "Fermi–Gaussian" phase shift functions considered in Fig. 7.10.

for X_{Fg}:

$$S(q) \simeq 2\left|\,\mathrm{Im}\left\{b_x^{(s,\beta)} + \beta\left(\frac{2A_{\mathrm{Fg}}}{q b_x^{(s,\beta)}}\right)^{1/2}\right\}\right|, \tag{7.86}$$

(for purely imaginary A_ℓ and A_{Fg}). For the logarithmic phase shift function the asymptotic value of the slope,

$$S(q) \simeq 2|\,\mathrm{Im}\, b_x^{(s,\beta)}| = 2\,\mathrm{Im}\sqrt{c^2 + i\pi\beta^2}, \tag{7.87}$$

is approached more rapidly than for the "Fermi–Gaussian". We note that the correction term for the "Fermi–Gaussian", proportional to $q^{-1/2}$, tends to reduce the slope. This explains why, at large momentum transfers in Fig. 7.10, the envelope of the differential cross section for the "Fermi–Gaussian" phase shift falls less rapidly than that for the logarithmic one.

Finally, in Fig. 7.12, we compare the three potentials that correspond to the differential cross sections of Fig. 7.10. The potential $V_{\mathrm{Fg}}(r)$ that corresponds to $\chi_{\mathrm{Fg}}(b)$ has been determined from the Abel equation,

$$V_{\mathrm{Fg}}(r) = -\frac{2vA_{\mathrm{Fg}}}{\pi\beta^2}\int_0^\infty \mathrm{d}\xi\,\frac{\exp[(r^2 - c^2 + \xi^2)/\beta^2]}{\{1 + \exp[(r^2 - c^2 + \xi^2)/\beta^2]\}^2}, \tag{7.88}$$

while $V_g(r)$ and $V_l(r)$ are as given in Fig. 7.8. Since the parameters considered are such that the three phase shift functions agree at large b, the potentials will similarly agree at large radii, whereas they differ considerably in magnitude at small r.

We have seen above that the asymptotic theory enables us to determine important features of the diffractive pattern from properties of the phase shift function. In particular, we have seen that the analytic properties of the phase shift function (or of the potential), which are not apparent from simple graphs of these quantities, are of great importance at large momentum transfers.